

Fluid-fluid displacement in mixed-wet porous mediaAshkan Irannezhad ¹, Bauyrzhan K. Primkulov ², Ruben Juanes ², and Benzhong Zhao ^{1,*}¹*Department of Civil Engineering, McMaster University, Hamilton, Ontario L8S 4L8, Canada*²*Department of Civil and Environmental Engineering,**Massachusetts Institute of Technology, Cambridge, Massachusetts 02139, USA*

(Received 5 July 2022; accepted 20 December 2022; published 11 January 2023)

It is well known that wettability exerts fundamental control over multiphase flow in porous media, which has been extensively studied in uniform-wet porous media. In contrast, multiphase flow in porous media with heterogeneous wettability (i.e., mixed-wet) is less well understood, despite its common occurrence. Here, we study the displacement of silicone oil by water in a mostly oil-wet porous media patterned with discrete water-wet clusters that have precisely controlled wettability. Surprisingly, the macroscopic displacement pattern varies dramatically depending on the details of wettability alteration—the invading water preferentially fills strongly water-wet clusters but encircles weakly water-wet clusters instead, resulting in significant trapping of the defending oil. We explain this counterintuitive observation with pore-scale simulations, which reveal that the fluid-fluid interfaces at mixed-wet pores resemble an S-shaped saddle with mean curvatures close to zero. We show that incorporation of the capillary entry pressures at mixed-wet pores into a dynamic pore-network model reproduces the experiments. Our work demonstrates the complex nature of wettability control in mixed-wet porous media, and it presents experimental and numerical platforms upon which further insights can be drawn.

DOI: [10.1103/PhysRevFluids.8.L012301](https://doi.org/10.1103/PhysRevFluids.8.L012301)

Multiphase flow in porous media is of great importance in many natural and industrial settings, including water infiltration [1], enhanced oil recovery [2], geologic carbon sequestration [3], and electrochemical devices [4]. The displacement of one fluid phase by another in porous media has long been viewed through the lens of Lenormand's diagram, which states that the flow behavior is governed by the viscosity ratio between the fluids, and the relative importance between capillary and viscous forces [5]. Concurrent studies [6,7] demonstrated that the fluids' relative affinity to the porous media (i.e., wettability) also has a profound influence on the flow behavior. Specifically, the displacement of a less wetting fluid by a more wetting fluid (i.e., imbibition) yields more compact displacement patterns compared to the displacement of a more wetting fluid by a less wetting fluid (i.e., drainage). More recently, a systematic study of fluid-fluid displacement in microfluidics [8] illustrated wettability control over a wide range of wettability conditions, which culminated in the extension of Lenormand's diagram to include wettability [9]. A common theme between these studies is the spatial uniformity of the porous media's wettability. In contrast, multiphase flow in porous media with a spatially heterogeneous wettability (i.e., mixed-wet) condition is less well understood.

Mixed-wet porous media is a common occurrence in many settings—for example, parts of a groundwater aquifer become water-repellent after contacting a nonaqueous phase liquid (NAPL) [10], and portions of a gas diffusion layer become water-repellent after the addition of polytetrafluoroethylene (PTFE) [11]. Mixed wettability is particularly prevalent in oil-bearing

*robinzhao@mcmaster.ca

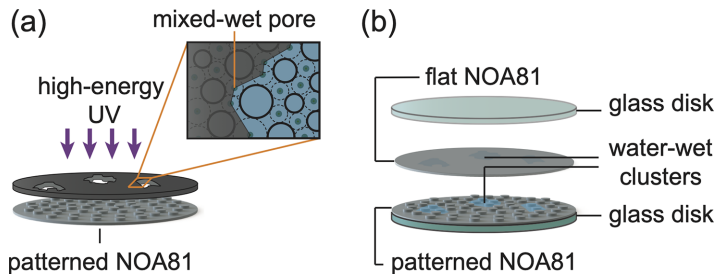


FIG. 1. We conduct radial fluid-fluid displacement experiments in microfluidic flow cells with spatially heterogeneous wettabilities. (a) The flow cell is made of a photocurable polymer (NOA81) that is oil-wet in nature, but becomes more water-wet after exposure to high-energy UV radiation. We cover the NOA81 surface with a photomask during UV exposure to achieve water-wet clusters. The borders between oil-wet and water-wet regions are delineated by connecting the centers of mixed-wet pores (inset). (b) The top half of the flow cell consists of a flat sheet of NOA81 patterned with the same spatially heterogeneous wettability and it is precision aligned with the bottom half.

reservoir rocks [12,13]. High-resolution *in situ* wettability characterizations of reservoir rocks demonstrated the presence of a wide range of contact angle within a single millimeter-sized core sample, and the existence of distinct water-wet and water-repellent regions [14–16].

Recent experiments in mixed-wet reservoir rocks demonstrated significant differences in flow behavior compared to their homogeneously wet counterparts. For instance, imbibition in an oil-saturated mixed-wet core sample displaced more oil [17–19], and imbibition in a CO₂-saturated mixed-wet core sample resulted in less residual trapping [20,21]. Additional features of multiphase flow in mixed-wet core samples include increases in ganglion flow [22,23] and the presence of fluid-fluid interfaces with a very low mean curvature [17,19].

Here, we use patterned microfluidic flow cells to study the viscously unfavorable displacement of silicone oil by water in mixed-wet porous media. This system allows for the simultaneous visualization of a macroscopic displacement front and the pore-scale fluid-fluid interface. Additionally, the flow cells are designed with precise pore geometries and mixed wettabilities in the form of discrete water-wet clusters, which eliminate the uncertainty associated with natural media and enable the direct mapping of observations to the interfacial fluid dynamics at the pore scale. Our results show that the macroscopic displacement pattern is sensitive to the exact wettability of the water-wet clusters—while the invading water preferentially fills *strongly water-wet clusters*, it encircles *weakly water-wet clusters* instead and traps a significant amount of the defending oil. We show that this dramatic difference is caused by the unique morphology of the fluid-fluid interface in mixed-wet pores, which resembles an S-shaped saddle with mean curvature close to zero. The pore-scale fluid-fluid interfaces dictate the capillary entry pressures, which lead to the preferential filling of mixed-wet pores over *weakly water-wet pores*, but not *strongly water-wet pores*. We incorporate the pore-scale insights into a dynamic pore-network model, which reproduces the experiments across different flow rates and wettability conditions.

Experiments in mixed-wet microfluidics. We conduct fluid-fluid displacement experiments in microfluidic flow cells with spatially heterogeneous wettability conditions (i.e., mixed-wet). Each flow cell contains ~ 16000 cylindrical posts and it is fabricated with a photocurable polymer (NOA81, Norland Optical Adhesives) [24]. The NOA81 surface is oil-wet in nature, but becomes increasingly water-wet with exposure to high-energy UV irradiation [8,25–27]. We expose the flow cell locally to high-energy UV via the application of a UV-blocking mask. The mask is patterned with cutouts that yield four distinct water-wet clusters [Fig. 1(a)]. We characterize the wettability of the flow cell using the static advancing contact angle θ of water immersed in silicone oil. The bulk of the flow cell is oil-wet ($\theta = 120^\circ$), while the clusters are either weakly water-wet ($\theta = 60^\circ$) or strongly water-wet ($\theta = 30^\circ$). We fabricate a new flow cell for each experiment to ensure precise

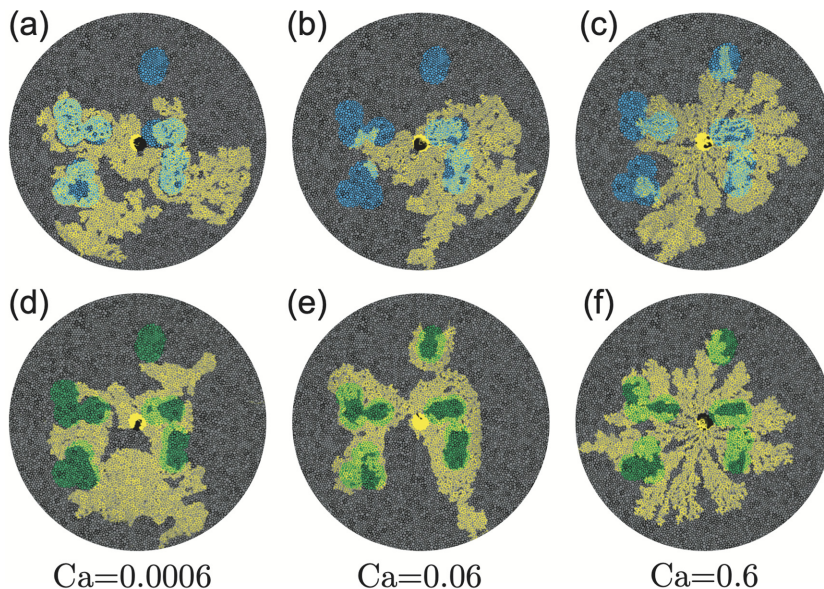


FIG. 2. Experimental displacement patterns of water (yellow) displacing silicone oil (black) in mixed-wet microfluidic flow cells at three distinct capillary numbers. The bulk of the flow cell is oil-wet (gray posts, $\theta = 120^\circ$), and it is interspersed either with strongly water-wet clusters (blue posts, $\theta = 30^\circ$), or with weakly water-wet clusters (green posts, $\theta = 60^\circ$). The patterns correspond to when the invading water reaches the perimeter of the flow cell and they are oriented in the same way to aid visual comparison. The invading water saturates the strongly water-wet clusters (top row), but encircles the weakly water-wet clusters (bottom row).

control over its wettability [Fig. 1(b)]. Furthermore, the wettability condition of the flow cell remains constant over the duration of our experiments, since the contact angle of the UV-treated NOA81 surface is stable over many days [25].

To perform an experiment, we first saturate the flow cell with a viscous silicone oil ($\eta_{\text{oil}} = 50$ mPa s). We then inject de-ionized water ($\eta_{\text{water}} = 0.99$ mPa s) into the center of the flow cell at a constant volumetric rate Q to displace the ambient silicone oil [Fig. 1(c)]. This is a viscously unfavorable displacement, with a viscosity ratio $\mathcal{M} = \eta_{\text{oil}}/\eta_{\text{water}} \approx 50$. We characterize the relative importance between viscous forces and capillary forces using the macroscopic capillary number $\text{Ca} = \eta_{\text{oil}} v_{\text{inj}}/\gamma$ [5], where $\gamma = 13 \pm 2$ mN/m is the interfacial tension between the fluids and $v_{\text{inj}} = Q/(bd)$ is the characteristic injection velocity as constrained by the gap thickness b and the median pore-throat size d . We conduct experiments at varying injection rates ($Q = 0.0003$, 0.03 and 0.3 mL/min), which correspond to capillary numbers spanning three orders of magnitude ($\text{Ca} = 6 \times 10^{-4}$, 6×10^{-2} , and 6×10^{-1} , respectively) for both types of mixed-wet flow cells. We provide a detailed description of the fabrication process and the experimental procedure in the Supplemental Material [28].

Intuitively, one would expect that the invading water preferentially fills the water-wet clusters in its path, especially at low Ca where capillary forces dominate. This is indeed the case for experiments in the mixed-wet flow cells with *strongly water-wet clusters* [Figs. 2(a)–2(c), and Movie S1 in the Supplemental Material [28]]. Surprisingly, we observe the opposite behavior in the mixed-wet flow cells with *weakly water-wet clusters*, where the water advances by encircling the weakly water-wet clusters instead of saturating them [Figs. 2(d)–2(f), and Movie S2 in the Supplemental Material [28]].

To provide quantitative insight into fluid-fluid displacement through the water-wet clusters, we calculate two metrics for each experiment: (i) The water-wet pore preference index I_p is the ratio of the number of invaded water-wet pore throats to the number of invaded mixed-wet pore throats

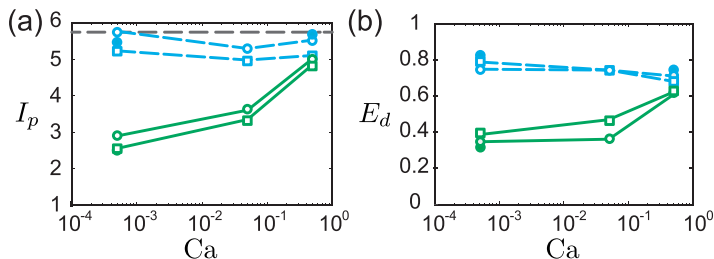


FIG. 3. (a) Water-wet pore preference index I_p as a function of Ca , where I_p is defined as the ratio between the number of invaded water-wet pore throats and the number of invaded mixed-wet pore throats. Experimental I_p for flow cells with weakly water-wet clusters (green circles connected by solid lines) and strongly water-wet clusters (blue circles connected by dashed lines) are plotted alongside numerical I_p (squares) obtained from our pore-network model (see Fig. 6). The gray dashed line represents the ratio between the total number of water-wet pore throats and the total number of mixed-wet pore throats in the entire flow cell. (b) Water-wet cluster displacement efficiency E_d as a function of Ca , where E_d is defined as the fraction of the defending fluid displaced from the water-wet cluster closest to the injection port. E_d for flow cells with weakly water-wet clusters (green circles connected by solid lines) and strongly water-wet clusters (blue circles connected by dashed lines) are plotted alongside numerical E_d (squares) obtained from our pore-network model (see Fig. 6). In both plots, the solid circles represent additional experiments conducted at the same conditions.

at the end of the experiment [Fig. 3(a)]. We define a mixed-wet pore throat as one that is between an oil-wet post and a water-wet post [Fig. 1(a)]. (ii) The water-wet cluster displacement efficiency E_d is defined as the fraction of the defending fluid displaced from the water-wet cluster closest to the injection port at the end of the experiment [Fig. 3(b)]. We confine E_d measurements to the water-wet cluster closest to the injection port because not all water-wet clusters come in the path of the invading water during the experiment.

We calculate the ratio between the total number of water-wet pore throats and the total number of mixed-wet pore throats in the entire flow cell as the upper bound for I_p (i.e., $I_p^{\max} = 5.8$), which correspond to the case where all encountered water-wet clusters are completely saturated by the invading water. We find a high water-wet pore preference index ($I_p > 5$) in the flow cell with strongly water-wet clusters at all Ca . Decreasing the affinity of the water-wet clusters to the invading fluid (i.e., increasing θ from 30° to 60°) dramatically decreases I_p . This is especially distinct at low Ca ($I_p < 3$), where the invading water enters the mixed-wet pore throats along the perimeter of the water-wet clusters without saturating them [Figs. 2(d) and 2(e)]. However, I_p in the flow cell with weakly water-wet clusters does increase at high Ca , when viscous forces become more important compared to capillary forces [Fig. 3(a)]. Similar observations have been reported by Armstrong and Wildenschild [29], whose x-ray computed microtomography (micro-CT) imaging of water flooding in oil-saturated mixed-wet cores showed that fluid-fluid interfaces are preferentially located in the mixed-wet pores.

At low Ca , the displacement efficiency is much higher in the flow cell with strongly water-wet clusters ($E_d = 0.78$) compared to the flow cell with weakly water-wet clusters ($E_d = 0.38$), since the preferential filling of mixed-wet pores along the perimeter of the weakly water-wet clusters traps a significant amount of the defending oil. As Ca increases, E_d decreases in the flow cell with strongly water-wet clusters as a result of viscous fingering. In contrast, E_d increases in the flow cell with weakly water-wet clusters. We find similar E_d values between the two types of mixed-wet flow cells at the highest Ca , where viscous forces dominate [Fig. 3(b)].

Pore-scale physics. The significant I_p and E_d differences between flow cells with strongly water-wet clusters and those with weakly water-wet clusters at low Ca indicate that capillarity at mixed-wet pores play a fundamental role. To gain a deeper understanding of wettability control at the pore scale, we investigate the fluid-fluid interface using SURFACE EVOLVER, which is a finite-element solver that minimizes the overall surface energy of a fluid-fluid-solid system [30]. Specifically,

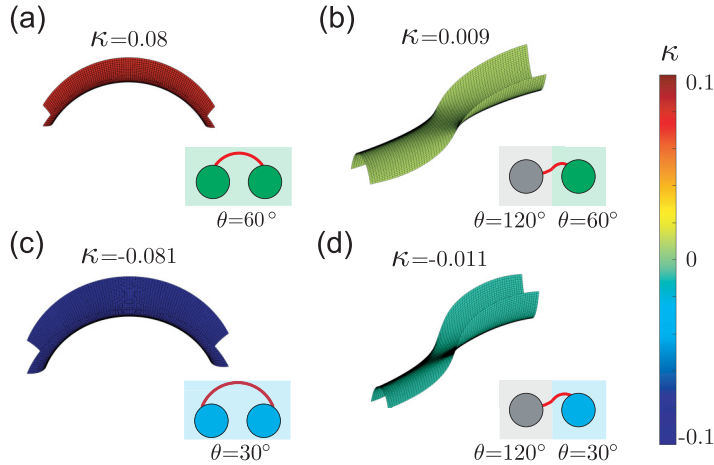


FIG. 4. Three-dimensional visualization of the last stable fluid-fluid interface through (a) a uniform-wet pore consisting of a pair of weakly water-wet posts, (b) a mixed-wet pore consisting of an oil-wet post next to a weakly water-wet post, (c) a uniform-wet pore consisting of a pair of strongly water-wet posts, and (d) a mixed-wet pore consisting of an oil-wet post next to a strongly water-wet post. The color map shows the local mean curvature of the meniscus.

we simulate the quasistatic evolution of the fluid-fluid interface in three dimensions (3D) through a typical uniform-wet pore throat versus a typical mixed-wet pore throat. Mixed-wet pore throats exist between a water-wet post and an oil-wet post, and we assign the wettability of the top and bottom surfaces such that the boundary between water-wet and oil-wet regions bisect the pore throat, which is similar to the experimental configuration [Fig. 1(a) inset]. We report the 3D shape of the last stable fluid-fluid interface, which occurs at the point beyond which no viable solution is possible (Fig. 4). Due to the equilibrium condition, each fluid-fluid interface has constant mean curvature κ in space.

The morphologies of fluid-fluid interfaces at mixed-wet pore throats are distinct from those at uniform-wet pore throats. Specifically, the fluid-fluid interfaces at mixed-wet pore throats resemble an S-shaped saddle with mean curvatures close to zero [Figs. 4(b) and 4(d)]. Pore-scale imaging of our experiments indeed shows the existence of S-shaped fluid-fluid interfaces at mixed-wet pore throats [Fig. 5(c)]. We note that saddle-shaped fluid-fluid interfaces with zero mean curvature have recently been observed in x-ray micro-CT imaging of waterflooding in oil-saturated Bentheimer sandstone cores [17]. For the flow cell with *weakly water-wet clusters*, the mean curvature of the fluid-fluid interface at a mixed-wet pore throat is lower than that at a uniform-wet pore throat [Figs. 4(a) and 4(b)]. Since capillary entry pressure is given by $P_c = \gamma\kappa$, the lower mean curvature is responsible for the preferential filling of mixed-wet pore throats in weakly water-wet clusters. For the flow cell with *strongly water-wet clusters*, the mean curvature of the fluid-fluid interface at a mixed-wet pore throat is higher than that at a uniform-wet pore throat [Figs. 4(c) and 4(d)], which is responsible for the preferential filling of water-wet pores.

Numerical simulation of fluid-fluid displacement in mixed-wet porous media. Among different classes of computational approaches to simulate pore-scale fluid-fluid displacement in porous media, pore-network models stand out in their relative simplicity and low computational demand [31]. Additionally, the pioneering work of Cieplak and Robbins demonstrated that pore network models with interface tracking can capture the impact of wettability on the macroscopic displacement pattern [7,32]. To capture the pore-scale physics in our experiments, we derive analytical expressions for the fluid-fluid interface evolution through both uniform-wet and mixed-wet pore throats (Fig. 5; Fig. S4 [28]). This allows us to calculate the critical capillary pressure at each pore throat along the invasion front, which takes place when the fluid-fluid interface encounters a burst, touch, or overlap

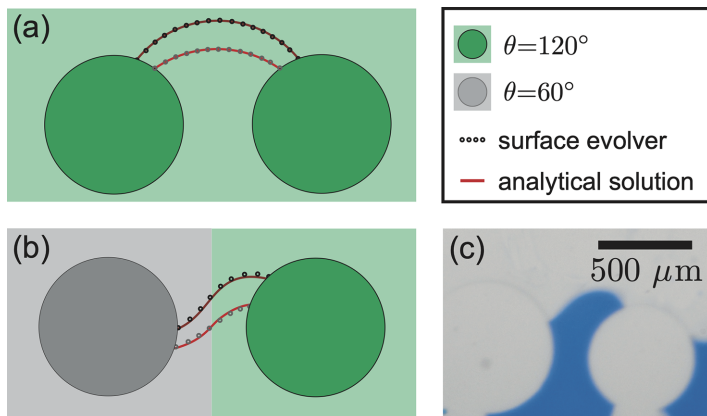


FIG. 5. In-plane curvature of the fluid-fluid interface at (a) a typical uniform-wet pore and (b) a typical mixed-wet pore. The circles represent simulation results obtained via SURFACE EVOLVER, whereas solid lines represent our analytical solutions [28]. (c) Experimental snapshot of the meniscus at a mixed-wet pore consisting of an oil-wet post next to a weakly water-wet post at $Ca = 6 \times 10^{-4}$.

event [7,32] (Fig. S5 [28]). Finally, we incorporate the critical capillary pressure in the dynamic pore-network model framework of Primkulov *et al.* [9,33,34] to arrive at a pore-scale model of fluid-fluid displacement in mixed-wet porous media.

We apply the pore-network model to simulate the constant rate displacement of silicone oil by water in our experiments (Fig. 6). Qualitatively, the simulations capture the salient features of the experiments—the invading water preferentially fills the *strongly water-wet clusters* but encircles the *weakly water-wet clusters* at low Ca . Quantitatively, the water-wet pore preference index I_p

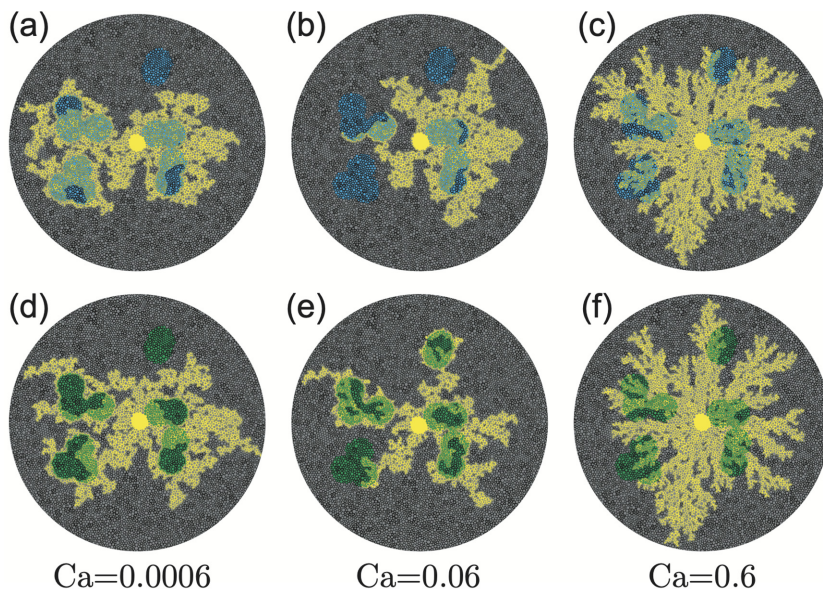


FIG. 6. Numerical displacement patterns simulated by the dynamic pore network model for the same conditions as the experiments. The simulations closely resemble the experiments (Fig. 2), and they capture the contrasting behaviors of water invasion in clusters of weakly water-wet posts vs clusters of strongly water-wet posts.

and water-wet cluster displacement efficiency E_d extracted from the simulations reproduce the experimental measurements across all Ca (Fig. 3).

We have developed a unique experimental platform to study multiphase flow in mixed-wet porous media via the displacement of silicone oil by water in predominantly oil-wet microfluidic flow cells patterned with well-controlled water-wet clusters. Our results show the macroscopic fluid-fluid displacement pattern is highly sensitive to the details of wettability alteration—while the invading water preferentially fills *strongly water-wet clusters*, it encircles *weakly water-wet clusters* instead and traps a significant amount of the defending oil (Fig. 2). This surprising finding stems from the unique morphology of the fluid-fluid interface in mixed-wet pores, which resembles an S-shaped saddle with mean curvature close to zero (Fig. 4). As a result, the critical capillary pressure of a typical mixed-wet pore is lower than that of a *weakly water-wet pore*, but higher than that of a *strongly water-wet pore*. We show that the pore-scale fluid-fluid interface at mixed-wet pores can be captured by simple analytical expressions (Fig. 5) and incorporated in a dynamic pore-network model, which reproduces our experimental observations across different wettability conditions and Ca (Fig. 6).

Our results highlight the nuanced, yet critical role wettability plays in multiphase flow in mixed-wet porous media. Meanwhile, the experimental and numerical platforms introduced here provide a controlled complement to traditional core-flooding experiments in natural porous media. These tools enable investigation of the many parameters that impact multiphase flow in mixed-wet porous media, including wettability contrast between clusters of different wetting properties, cluster size, and spatial distribution, to name a few.

Acknowledgments. The authors thank Doris Stevanovic at the McMaster Center for Emerging Device Technologies (CEDT) for her training and guidance on clean room equipment. This research was supported by the Natural Sciences and Engineering Research Council of Canada (NSERC) Discovery Grants.

-
- [1] L. Cueto-Felgueroso and R. Juanes, Nonlocal Interface Dynamics and Pattern Formation in Gravity-Driven Unsaturated Flow through Porous Media, *Phys. Rev. Lett.* **101**, 244504 (2008).
 - [2] F. M. Orr and J. Taber, Use of carbon dioxide in enhanced oil recovery, *Science* **224**, 563 (1984).
 - [3] M. L. Szulczewski, C. W. MacMinn, H. J. Herzog, and R. Juanes, Lifetime of carbon capture and storage as a climate-change mitigation technology, *Proc. Natl. Acad. Sci. USA* **109**, 5185 (2012).
 - [4] B. Zhao, C. H. Lee, J. K. Lee, K. F. Fahy, J. M. LaManna, E. Baltic, D. L. Jacobson, D. S. Hussey, and A. Bazylak, Superhydrophilic porous transport layer enhances efficiency of polymer electrolyte membrane electrolyzers, *Cell Rep. Physical Science* **2**, 100580 (2021).
 - [5] R. Lenormand, E. Touboul, and C. Zarcone, Numerical models and experiments on immiscible displacements in porous media, *J. Fluid Mech.* **189**, 165 (1988).
 - [6] J. P. Stokes, D. A. Weitz, J. P. Gollub, A. Dougherty, M. O. Robbins, P. M. Chaikin, and H. M. Lindsay, Interfacial Stability of Immiscible Displacement in a Porous Medium, *Phys. Rev. Lett.* **57**, 1718 (1986).
 - [7] M. Cieplak and M. O. Robbins, Dynamical Transition in Quasistatic Fluid Invasion in Porous Media, *Phys. Rev. Lett.* **60**, 2042 (1988).
 - [8] B. Zhao, C. W. MacMinn, and R. Juanes, Wettability control on multiphase flow in patterned microfluidics, *Proc. Natl. Acad. Sci. USA* **113**, 10251 (2016).
 - [9] B. K. Primkulov, A. A. Pahlavan, X. Fu, B. Zhao, C. W. MacMinn, and R. Juanes, Wettability and Lenormand’s diagram, *J. Fluid Mech.* **923**, A34 (2021).
 - [10] S. E. Powers, W. H. Anckner, and T. F. Seacord, Wettability of NAPL-contaminated sands, *J. Environ. Eng.* **122**, 889 (1996).
 - [11] P. K. Sinha and C.-Y. Wang, Liquid water transport in a mixed-wet gas diffusion layer of polymer electrolyte fuel cell, *Chem. Eng. Sci.* **63**, 1081 (2008).

- [12] R. A. Salathiel, Oil recovery by surface film drainage in mixed-wettability rocks, *J. Pet. Technol.* **25**, 1216 (1973).
- [13] A. R. Kovscek, H. Wong, and C. J. Radke, A pore-level scenario for the development of mixed wettability in oil reservoirs, *AIChE J.* **39**, 1072 (1993).
- [14] M. Andrew, B. Bijeljic, and M. Blunt, Pore-scale contact angle measurements at reservoir conditions using x-ray microtomography, *Adv. Water Resour.* **68**, 24 (2014).
- [15] A. AlRatrou, M. J. Blunt, and B. Bijeljic, Wettability in complex porous materials, the mixed-wet state, and its relationship to surface roughness, *Proc. Natl. Acad. Sci. USA* **115**, 8901 (2018).
- [16] M. J. Blunt, Q. Lin, T. Akai, and B. Bijeljic, A thermodynamically consistent characterization of wettability in porous media using high-resolution imaging, *J. Colloid Interface Sci.* **552**, 59 (2019).
- [17] Q. Lin, B. Bijeljic, S. Berg, R. Pini, M. J. Blunt, and S. Krevor, Minimal surfaces in porous media: Pore-scale imaging of multiphase flow in an altered-wettability Bentheimer sandstone, *Phys. Rev. E* **99**, 063105 (2019).
- [18] A. M. Alhammedi, Y. Gao, T. Akai, M. J. Blunt, and B. Bijeljic, Pore-scale X-ray imaging with measurement of relative permeability, capillary pressure and oil recovery in a mixed-wet micro-porous carbonate reservoir rock, *Fuel* **268**, 117018 (2020).
- [19] A. Scanziani, Q. Lin, A. Alhosani, M. J. Blunt, and B. Bijeljic, Dynamics of displacement in mixed-wet porous media, *Proc. R. Soc. A* **476**, 20200040 (2020).
- [20] A. S. Al-Menhali and S. Krevor, Capillary trapping of CO₂ in oil reservoirs: Observations in a mixed-wet carbonate rock, *Environ. Sci. Technol.* **50**, 2727 (2016).
- [21] A. S. Al-Menhali, H. P. Menke, M. J. Blunt, and S. C. Krevor, Pore scale observations of trapped CO₂ in mixed-wet carbonate rock: Applications to storage in oil fields, *Environ. Sci. Technol.* **50**, 10282 (2016).
- [22] S. Zou, R. T. Armstrong, J.-Y. Arns, C. H. Arns, and F. Hussain, Experimental and theoretical evidence for increased ganglion dynamics during fractional flow in mixed-wet porous media, *Water Resour. Res.* **54**, 3277 (2018).
- [23] M. Rücker, W. B. Bartels, K. Singh, N. Brussee, A. Coorn, H. A. van der Linde, A. Bonnin, H. Ott, S. M. Hassanizadeh, M. J. Blunt, H. Mahani, A. Georgiadis, and S. Berg, The effect of mixed wettability on pore-scale flow regimes based on a flooding experiment in Ketton limestone, *Geophys. Res. Lett.* **46**, 3225 (2019).
- [24] D. Bartolo, G. Degré, P. Nghe, and V. Studer, Microfluidic stickers, *Lab Chip* **8**, 274 (2008).
- [25] B. Levaché, A. Azioune, M. Bourrel, V. Studer, and D. Bartolo, Engineering the surface properties of microfluidic stickers, *Lab Chip* **12**, 3028 (2012).
- [26] B. Levaché and D. Bartolo, Revisiting the Saffman-Taylor Experiment: Imbibition Patterns and Liquid-Entrainment Transitions, *Phys. Rev. Lett.* **113**, 044501 (2014).
- [27] C. Odier, B. Levaché, E. Santanach-Carreras, and D. Bartolo, Forced Imbibition in Porous Media: A Fourfold Scenario, *Phys. Rev. Lett.* **119**, 208005 (2017).
- [28] See Supplemental Material at <http://link.aps.org/supplemental/10.1103/PhysRevFluids.8.L012301> for a detailed description of the microfluidic flow cell fabrication procedure, derivation of interface curvature at mixed-wet pores, and videos of the experiments and simulations.
- [29] R. T. Armstrong and D. Wildenschild, Microbial enhanced oil recovery in fractional-wet systems: A pore-scale investigation, *Transp. Porous Med.* **92**, 819 (2012).
- [30] K. A. Brakke, The surface evolver, *Exp. Math.* **1**, 141 (1992).
- [31] M. J. Blunt, Flow in porous media—pore-network models and multiphase flow, *Curr. Opin. Colloid Interface Sci.* **6**, 197 (2001).
- [32] M. Cieplak and M. O. Robbins, Influence of contact angle on quasistatic fluid invasion of porous media, *Phys. Rev. B* **41**, 11508 (1990).
- [33] B. K. Primkulov, S. Talman, K. Khaleghi, A. Shokri, R. Chalaturnyk, B. Zhao, C. W. MacMinn, and R. Juanes, Quasistatic fluid-fluid displacement in porous media: Invasion-percolation through a wetting transition, *Phys. Rev. Fluids* **3**, 104001 (2018).
- [34] B. K. Primkulov, A. A. Pahlavan, X. Fu, B. Zhao, C. W. MacMinn, and R. Juanes, Signatures of fluid-fluid displacement in porous media: Wettability, patterns and pressures, *J. Fluid Mech.* **875**, R4 (2019).